Journal of Applied Fluid Mechanics, Vol. 18, No. 6, pp. 1430-1445, 2025.
Available online at www.jafmonline.net, ISSN 1735-3572, EISSN 1735-3645.
https://doi.org/10.47176/jafm.18.6.3175

Effect of Disk Friction Loss Reduction on Flow Phenomena in Low-specific Speed Centrifugal Pump: An Experimental and Numerical Approach

D. Satish[1,2†], A. Doshi [1] and M. Bade [1]

[1] *Department of Mechanical Engineering, Sardar Vallabhbhai National Institute of Technology, Surat 395007, Gujarat, India*
[2] *Department of Mechanical Engineering, Sarvajanik College of Engineering and Technology, Surat 395001, Gujarat, India*

†*Corresponding Author Email:* satish.dokiparti@scet.ac.in

ABSTRACT

Disk friction loss (L_{DF}) plays an important factor in the performance of the low-specific speed (N_S) centrifugal pump. Reducing the rear axial clearance ($C_{s,a,r}$) is profound method to lower the L_{DF} and improve the efficiency of pump (η). In this research article, a low N_s = 19 rpm centrifugal pump was evaluated using computational fluid dynamics (CFD) and experimental analysis at different 1000, 900 and 800 rpms over a range of flow rates (Q). Two models: Model A with original $C_{s,a,r}$ of 23 mm and Model B with reduced $C_{s,a,r}$ of 1 mm were analyzed. To grasp the knowledge about internal flow physics, the pressure contours, velocity contours, velocity vectors and streamlines have been thoroughly studied. CFD results were found in good agreement with the experiments performed on the test setup. The experimental improvements in η at their respective best efficiency points (BEP) were determined to be 3.94%, 3.91%, and 2.81% for 1000, 900, and 800 rpms respectively. While an average 3.43%, 1.79% and 0.76% improvement in head (H) was obtained for 1000, 900, and 800 rpms respectively. Considering the lower disk friction coefficient (C_m) and power loss (P_L) due to L_{DF}, the Model B works optimum at higher rpm.

Article History

Received October 8, 2024
Revised December 27, 2024
Accepted January 6, 2025
Available online March 30, 2025

Keywords:

Low-specific speed pump
Disk friction loss
Clearance flow
CFD
Cavity filling ring

1. INTRODUCTION

Historical records indicate that Asian and other ancient civilizations have been using pumps since 1000 Before Common Era (BCE) (Wilson, 1982). In this regard, pumps can be regarded as among the first known techniques for transferring energy to fluids for transportation. The pump is a type of general rotating machinery used in many different industries, including water supply, water drainage, agricultural land irrigation, and so forth. To transfer the fluid a centrifugal pump uses the centrifugal force generated by the impeller's rotating motion. In addition to the water industries, centrifugal pumps are extensively utilized in the transportation of slurries containing solid particles in the coal industries, building industries, power generation industries, and other industries. Centrifugal pump manufacturing as well as research and development are also expanding quickly.

Among the all end user energy sectors, industries are the major energy consumer (~38% of total final consumption) and highest Carbon Dioxide (CO_2) emitter (~47% of total emission) by 2023 (IEA, 2023). Figure 1 depicts the industrial electricity demand in 2022 by various end users.

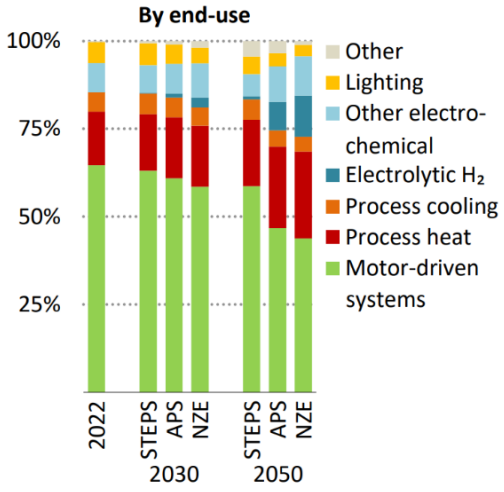

Fig. 1 Industrial electricity demand by various end users (IEA, 2023)

NOMENCLATURE

Acronyms

BCE	Before Common Era
BEP	Best efficient point
CFD	Computational fluid dynamics
CO_2	carbon dioxide
GCI	Grid Convergence Index
PLC	Programmable Logic Controller
RANS	Reynolds Average Navier-Stokes
SCADA	Supervisory Control And Data Acquisition
SST	Shear Stress Transport
TWh	tera watthours
VFD	Variable Frequency Drive

Symbols

C_m	disk friction coefficient
C_s	clearance space
N_s	specific speed
lps	liter per second
D	diameter of impeller
e	error
F	force
H	total head
L	losses
N	rotational speed
P	power
Q	flow rate
r	refinement factor
R	radius of impeller
T	torque
u	velocity
k	surface roughness

Greek Symbols

Δ	difference
η	overall efficiency
μ	viscosity
ρ	density
ω	angular velocity

Subscripts

h	hydraulic
DF	Disk Friction
EXP	experimental
a	axial
d	design
ext	extrapolated
$fine$	fine
max	maximum
min	minimum
r	rear

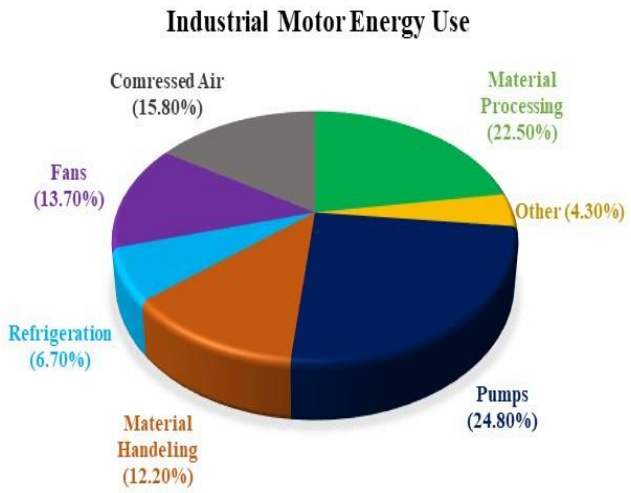

Fig. 2 Industrial motor-driven systems energy usage (reconstructed) (Ahmed & Creamer, 2024)

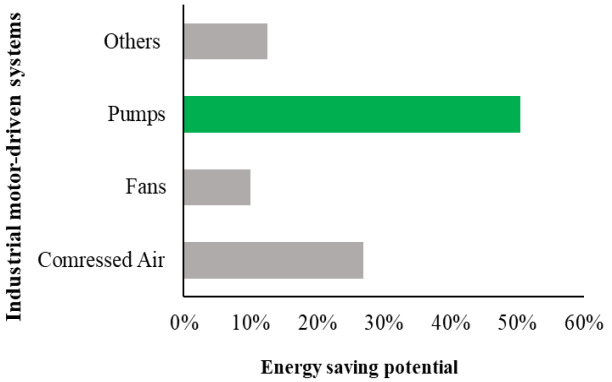

Fig. 3 Industrial motor-driven systems energy saving potential (reconstructed) (Ahmed & Creamer, 2024)

In modern industries, motor-driven devices consume about 65% of the electricity used in the sector in 2022. Over the past decade, electricity consumption by motor-driven devices has increased almost 60% (630 tera watthours [TWh]) and likely to be increase in future.

These motor-driven devices include various drives for pumps, fans, material handling, processing, compressed air systems, and other applications. As per Fig. 2, one can see that pumps accounts for more than 24% of the energy used by industrial motor-driven systems. Furthermore, over 50% of the potential energy savings from motor powered pumps can be attributed to duty cycle fluctuation, Affinity Laws, inherent losses, and frequent oversizing of pump systems as depicted in Fig. 3. This emphasizes how important it is to concentrate on increasing pump efficiency. The creation of a new generation of energy-efficient pumps and pump systems is greatly influenced by this energy saving potential. Even, various government and regulatory bodies are working on setting the standard for the advancement of energy-efficient pumps and energy savings.

Being an energy operated machine, the output of the centrifugal pump will be always less than the input power owing to the losses. As shown in Fig. 4, the pump losses are basically classified into two parts: (1) external losses and (2) internal losses. The mechanical losses accounts for the external losses which occur at the bearing and shaft seals due to the improper lubrication. These losses can be reduced by using the improved bearing. Internal losses are further divided into hydraulic losses and secondary losses.

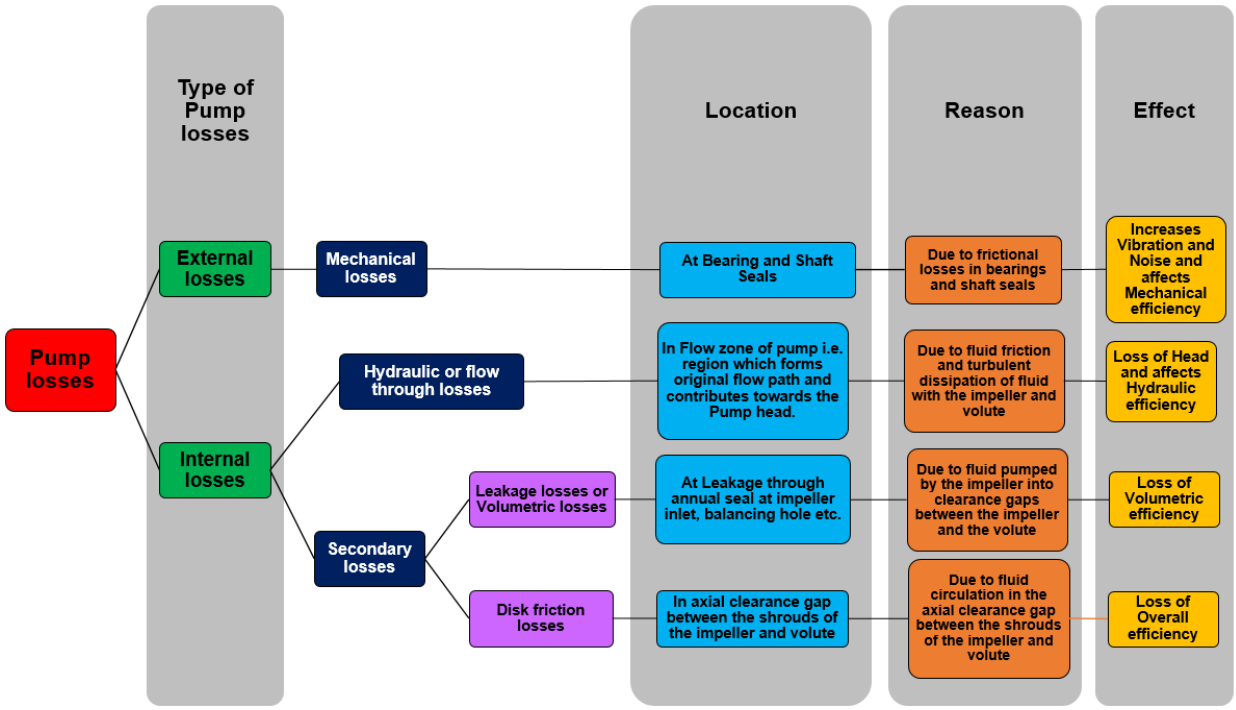

Fig. 4 Pump losses – location, reason and effect

The hydraulic losses develop in the flow zone of pump due to the fluid friction between impeller and volute. The secondary losses are sub divided into the leakage loses due to the seal leakage and disk friction losses (L_{DF}) due to the axial clearance space ($C_{s,a}$) between the shrouds of the impeller and volute (Gülich, 2019). To reduce the hydraulic losses and leakage losses one needs to use highly smoothed impeller and volute. The location of each loss in pump where it occurred, the reason and its contribution in various types of losses are mentioned in Fig. 4. All the methods applied to reduce the mechanical as well as, hydraulic and leakage losses will add more cost and requires major modification in existing design of pumps. Gülich (2003) research highlights that L_{DF} have a significant impact on the efficiency of centrifugal pumps having low or moderate-specific speed (N_s). For a low-specific speed pump (N_s = 10 rpm), power loss (P_L) due to L_{DF}, typically accounted for about 50% of the useful power, whereas for high-specific speed pump (N_s = 30 rpm), this fraction was reduced to approximately 5%. Hence, further studies need to be done to reduce the L_{DF} on a pump having low N_s.

Various reserachers have tried to improve the performance of centrifugal pump by varying the geometry of the impeller (Iversen, 1955; Shimosaka, 1959; Raheel & Engeda, 2005); profile, angle and geometry of blades (Shirinov & Oberbeck, 2011a, b; Choi et al., 2013; Chen et al., 2024); geometry of side channels as well as other geometrical parameters. A very few authors have explored the impact of reducing C_s on L_{DF} (Sixsmith, 1913; Badami, 1997; Raheel & Engeda, 2005; Horiguchi et al., 2008). Will et al. (2012) experimentally and numerically studied the flow dynamics of a moderate-specific speed (N_s = 22.8 rpm) centrifugal pump using balancing holes. Their study found that balancing holes reduces the pressure gradients and axial force ($F_{a,r}$) by introducing centripetal inward flow, which diminishes recirculation in the rear axial clearance space ($C_{s,a,r}$). Ayad et al. (2015) investigated the effect of $C_{s,a,r}$ on a specific speed (N_s = 28.7 rpm) centrifugal pump performance using numerical simulations. They found that reducing $C_{s,a,r}$ by 3 mm improves the head (H) from 3.15 m to 5.9 m, overall efficiency (η) from 40% to 47% and slip factor from 0.7 to 0.84. Similarly, Cao et al. (2015) studied the effects of varying $C_{s,a,r}$ by 0.20 mm for a centrifugal pump of N_s = 45.2 rpm through model tests and simulations. Simulation results show that for each increment of 0.20 mm in $C_{s,a,r}$, reduces η by 4.67%. Pehlivan and Parlak (2019) simulated the effect of $C_{s,a,r}$, wear ring and balancing holes on a single suction closed centrifugal pump with N_s = 22.6 rpm. Compared to the 51.5% η_o at 40 mm $C_{s,a,r}$, the rise in η_o of 46.2% was obtained at 5 mm $C_{s,a,r}$. Adistiya and Wijayanta (2019) demonstrated that $C_{s,a,r}$ directly influences recirculation flow within a pump, affecting rotor stability, shaft integrity, and overall performance. Their calculations revealed that reducing $C_{s,a,r}$ from 0.02025 inches to 0.020 and 0.019 inches improved hydraulic efficiency (η_h) from 28% to 29% and 36%, respectively, highlighting that smaller $C_{s,a,r}$ enhances the hydraulic performance. Streamline and pressure distribution in a N_s = 24.7 rpm centrifugal pump for with and without $C_{s,a,r}$ were examined using k-ω turbulence model by Zheng et al. (2020). In the volute, reducing the $C_{s,a,r}$ led to a lower pressure with a decrease in pressure fluctuation amplitude by 56.38% to 65.34%. Inaba et al. (2021) investigated the effect of narrowing $C_{s,a,r}$ and reducing L_{DF} on flow structure of centrifugal pump impeller using experimental and computational approach. Each approach supports that the vortex in the $C_{s,a,r}$ has a remarkable effect on reducing the L_{DF} under slightly

inward flow conditions. Jin et al. (2022) examined the influence of $C_{s,a}$, flow rate (Q) and impeller rotational speed (N) on L_{DF} using $F_{a,r}$ for a centrifugal pump (N_s = 23.4 rpm). The outcome indicates that by reducing the $C_{s,a}$ from 0.5 mm to 0.1 mm, it lowers the L_{DF} as $F_{a,r}$ increases by nearly 74%. Peng et al. (2022) studied the effect of varying $C_{s,a,r}$ (0.10, 0.22, 0.42 and 0.62 mm) on hydraulic performance of N_s = 45.2 rpm centrifugal pump. Results found from the numerical simulations indicates that reducing $C_{s,a,r}$ from 0.62 mm to 0 mm, leakge flow rate from the volute into the front pump cavity reduces by 52.87% and from the front pump cavity back to the impeller inlet by 66.21%. The volumetric loss performance numerical analysis of a low-specific speed (N_s = 18.2 rpm) pump was done by Kim et al. (2023) using water as well as various viscosity crude oils for varying $C_{s,a,r}$ from 0.25 to 1.00 mm. Volumetric loss decreases with smaller $C_{s,a,r}$, dropping from 0.0023 kg/s at 1 mm to 0.0015 kg/s at 0.25 mm for viscous fluids. To assess L_{DF} and internal flow of the clearance flow channel, Maeda et al. (2024) numerically investigated the clearance flow channel, which replicates the clearance flow on the rear of the centrifugal impeller by utilizing rotating disks in a closed chamber. Results showed that the fin reduced L_{DF} by separating the clearance flow and increasing circumferential velocity.

The available literature highlights the importance of pump performance improvement by reducing the L_{DF} by lowering the $C_{s,a,r}$. Although, these numerical as well as experimental research is mainly concentrated on higher N_s pumps. Experimental investigation of low-specific speed N_s pumps are very rare in literature. Further, To the best of the authors' knowledge, none of them offered techniques that could be simply integrated into current low-specific speed N_s pump designs without requiring major adjustments. Hence, the main aim of this research is to investigate the effect of reduction in L_{DF} for low-specific N_s pump by reducing the $C_{s,a,r}$. In this research article, two models were considered for Computational Fluid Dynamics (CFD) and experimental analysis: Model A with original $C_{s,a,r}$ of 23 mm and Model B with reduced $C_{s,a,r}$ of 1 mm. A low-specific speed (N_s = 19 rpm) pump was evaluated at different rpms (1000, 900 and 800 rpm) and various flow rates for both the models. The article is arranged as follows: Section 2 provides the CFD simulation methodology and results for both the models. Section 3 represents the experimental procedure, description of experimental test setup and instruments used during experiments, while Section 4 compares and validates the CFD and experimental results. The overall finding in terms of the conclusion is presented in Section 5 along with the scope of future work.

2. CFD SIMULATION ANALYSIS

2.1 Geometry of the Centrifugal Pump

In this numerical investigation, a low-specific speed (N_s = 19 rpm) single stage centrifugal pump shown in Fig. 5 is used. This centrifugal pump has design flow rate (Q_d) of 17.5 lps, head (H_d) of 21 m and speed (N_d) of 1450 rpm. The selected pump has single axial suction as well as vane less volute having inlet diameter of 67 mm. The impeller has inlet diameter of 100 mm and outlet diameter of 260 mm with 15.5 mm impeller width. The 5 mm thick shroud of the impeller was machined. The five backwards curved blades with 3.4 mm thickness are at 21.7° inlet angle. The electric motor of 11 kW and 2905 rpm was used to drive the pump.

Fig. 5 Geometry of the analyzed centrifugal pump

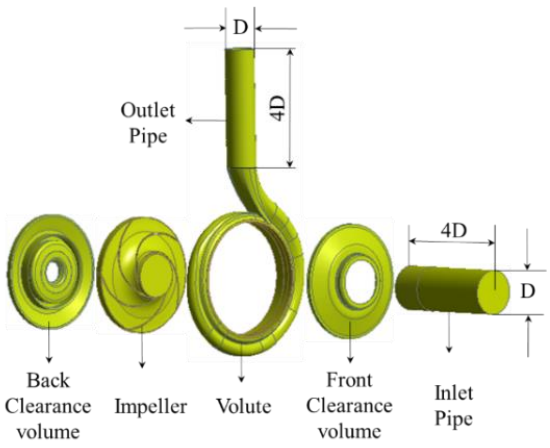

Fig. 6 Computational fluid model of centrifugal pump

2.2 Computational Model and Mess Generation

Using the Ansys Workbench® the computational fluid model of selected pump was designed as shown in Fig. 6. The designed computational model consists of volute, front clearance volume, back clearance volume, impeller and inlet as well as outlet pipe. General industrial practice suggest that the inlet and outlet pipe length should be four times of the diameter of the impeller (D) to ensure the flow stability at pump inlet and pump outlet in CFD simulations. If the sufficient lengths are not taken then in simulations sudden abrupt flow changes will be observed and it will not give the clear idea of the flow analysis (Ayad et al., 2015; Cao et al., 2015; Zheng et al., 2020; Zhu et al., 2012). The geometry of the original pump was modelled using the available technical specifications. To identify the effect of lowering the $C_{s,a,r}$ on the L_{DF}, two different models were analyzed: Model A with original $C_{s,a,r}$ (23 mm) and model B with reduced $C_{s,a,r}$ (1 mm) as shown in Fig. 7. To minimize the L_{DF}, a specially designed cavity filling ring shown in Fig. 8 is used to reduce the gap between the back cover plate and back shroud which minimizes the $C_{s,a,r}$. The cavity filling ring is modelled based on the shape and geometry of the back axial clearance between back cover plate and back shroud.

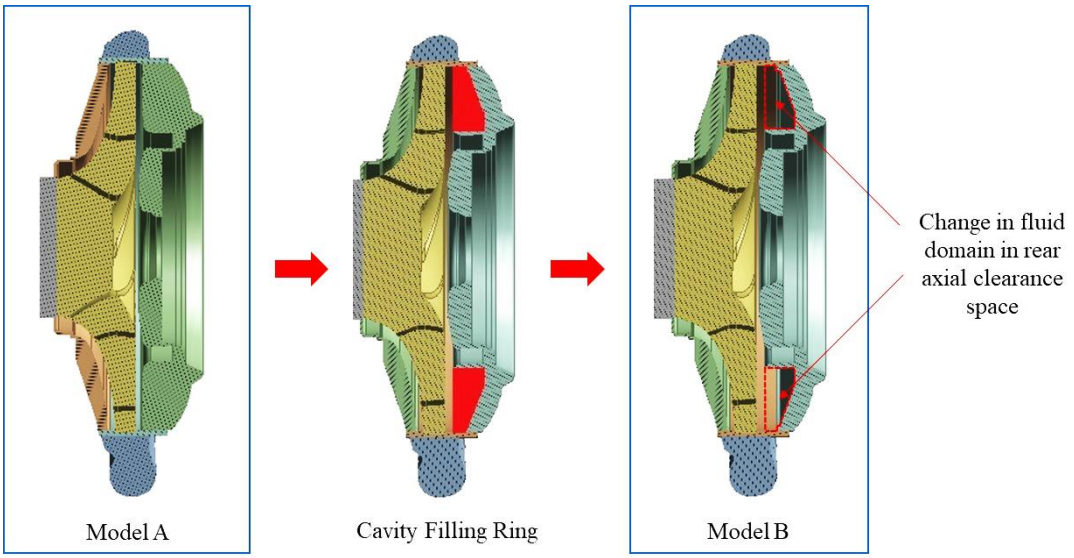

Fig. 7 Computational fluid model of centrifugal pump for Model A and Model B

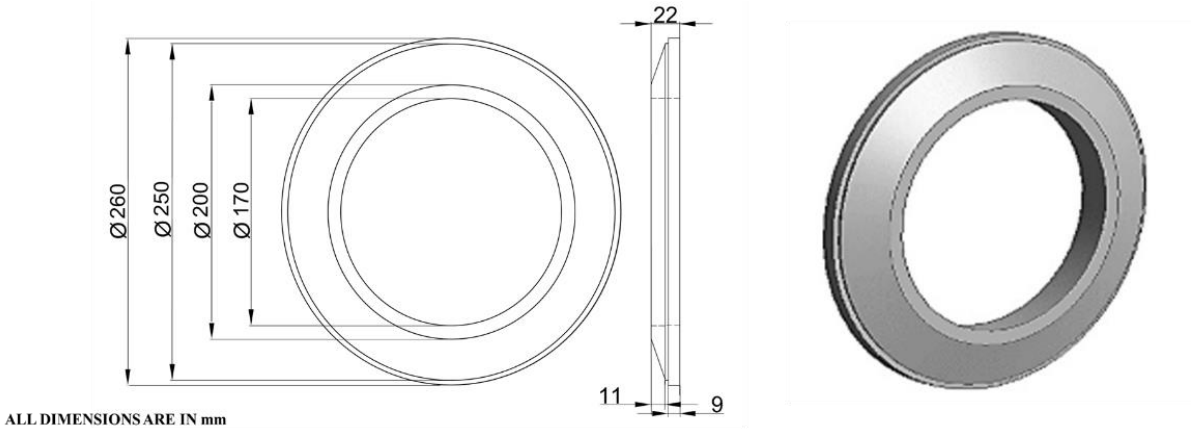

(a) (b)

Fig. 8 Cavity filling ring (a) geometrical dimensions (b) computational model

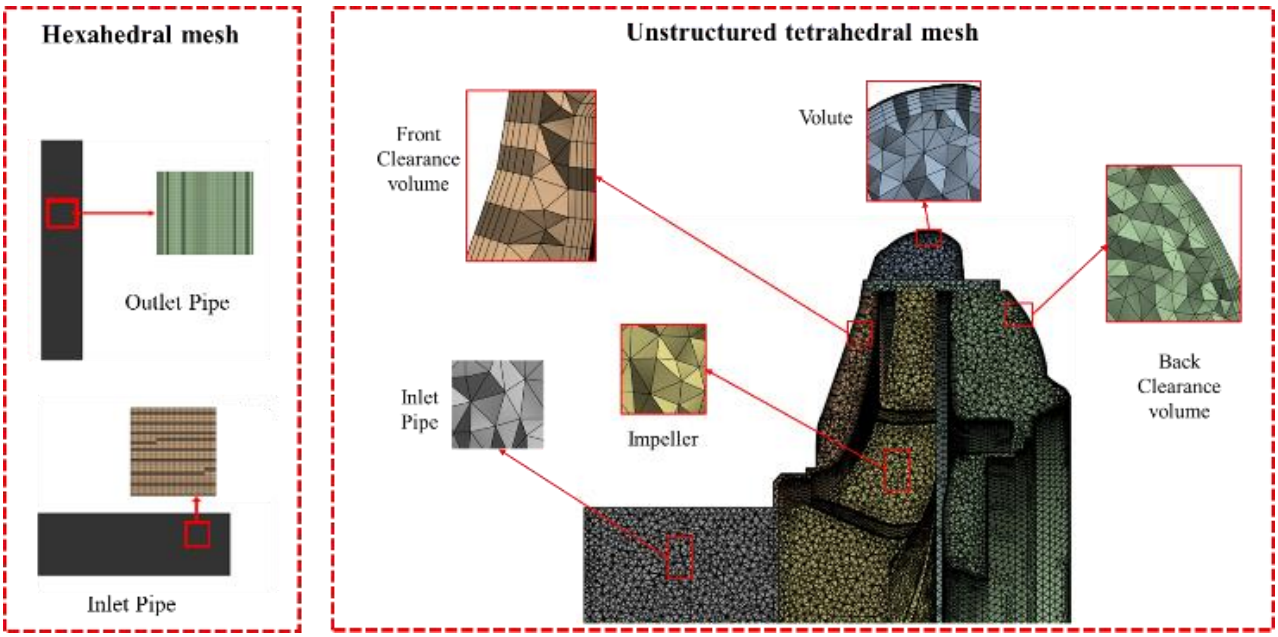

Fig. 9 Unstructured tetrahedral and hexahedral mesh used for meshing the flow domain

Considering the complex geometry of the problem, an unstructured tetrahedral mesh was used for the impeller, volute and cavity filling ring volume, while unstructured hexahedral mesh was used for the inlet as well as outlet pipe regions as shown in Fig. 9. Mesh quality was verified using the aspect ratio and orthogonal quality techniques for accurate results. The unstable three-dimensional incompressible Reynolds-averaged Navier-Stokes equations (RANS) served as the governing equations. The following is the primary format for governing equations:

$$\frac{\partial u_i}{\partial x_i} = 0 \tag{1}$$

$$\frac{\partial}{\partial t}(\rho u_i) + \frac{\partial}{\partial x_j}(\rho u_i u_j) = -\frac{\partial \rho}{\partial x_i} + \frac{\partial}{\partial x_j}\left(\mu \frac{\partial u_i}{\partial x_j}\right) + S_i \tag{2}$$

where x_i is the components in i direction, u_i are the average velocity components in i direction, S_i is the source term. As per the research done by Wilcox (1994; 1988), the $k-\omega$ model assumes that the turbulence viscosity μ, is function of the turbulence kinetic energy k and turbulent frequency ω as below:

$$\mu = \rho \frac{k}{\omega} \tag{3}$$

Under the isothermal conditions of 25°C, the CFD analysis was carried out with water as fluid. The multi-reference frame technique was used with impeller in rotating reference frame and volute with other domains in fixed reference frame. The Frozen Rotor quasi-steady algorithm with 360° pitch angle on both sides of the interface was used to connect these frames. The $k-\omega$ Shear stress transport (SST) model in ANSYS CFX was employed to solve the RANS equations due to faster convergence and good agreement with the experimental results. In addition, the resolution of the near wall for low Reynolds flows number is a benefit of the conventional $k-\omega$ model. Because it does not depend on the intricate non-linear damping functions needed for the conventional $k-\varepsilon$ model, it is also more accurate and stable (Osman et al., 2022). At the inlet of the pipe mass flow rate and at the exit of the outlet pipe static pressure was defined. The empirical value of 5% turbulence intensity was considered. Under the no slip conditions for wall boundaries, the convergence criterions were set to RMS 10-5. For the accurate selection of grid scheme, the grid convergence index (GCI) method is used to check the convergence of the grids (Abernethy et al., 1985; Celik et al., 2021; Li et al., 2023). Total three groups of grid schemes with grid element numbers 2.2 x 10^6, 0.62 x 10^6 and 0.14 x 10^6 were taken with corresponding shaft power characteristics parameters. The grid refinement factor (r_{21} and r_{32}) between the grid schemes is 1.106 and 1.156, respectively. Taking the shaft power as evaluation criteria, the extrapolated relative error (e_{ext}^{21}) is 0.011% and fine GCI (GCI_{fine}^{21}) is 1.394%. Hence, 2.2 x 10^6 grid element numbers are selected due to the discrete errors in the grid. In addition to minimize the computation time, the mesh/grid independency test was performed for Model A at 1000 rpm and highest efficiency point to determine the optimum number of mesh elements as shown in Fig. 10. The number of mesh elements was ranged in 0.15 million to 3.03 million. For the evaluation criterion, the mean difference of H and η was considered. At last, the 2.2 million number of dependent mess elements and corresponding mesh size were selected for which the mean difference of H and η was within ±1%.

3. EXPERIMENTAL METHODOLOGY

3.1 Fabrication of Model B

For Model B, a cavity filling ring manufactured using the dimensions and shape as shown in Fig. 8 was applied

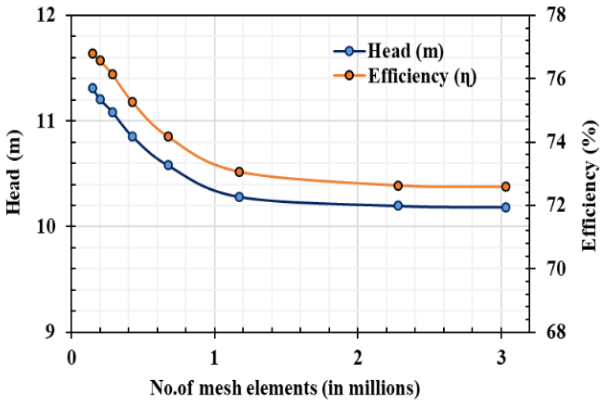

Fig. 10 Mesh/grid independency

to Model A. This cavity filling ring was attached on the back cover plate of the pump which lowers the $C_{s,a,r}$ to 1 mm from 23 mm in Model A. This ring design varies from the pump to pump as the shape and size of the $C_{s,a,r}$ between back shroud and back cover plate depends on the volute and impeller geometry of the pump as well as challenges associated with the manufacturing. The manufactured cavity filling ring is shown in Fig. 11 (a), while its attachment on back cover plate is shown in Fig. 11 (b). Wood was selected to fabricate the filling ring as it is easy to manufacture and can be easily fitted on back cover plate using simple joints. In addition, it provides comparatively smooth surface without disturbing the dynamic operations of the pump at lower cost.

3.2 Overview of the Experimental Test Set Up and Data Collection

The experiments were carried out on an open-loop type test bench, as shown in Fig. 12. This test bench was established to investigate the hydraulic and dynamic performance of the centrifugal pumps at the Fluid Mechanics and Fluid Machine Laboratory, Sardar Vallabhbhai National Institute of Technology, Surat as

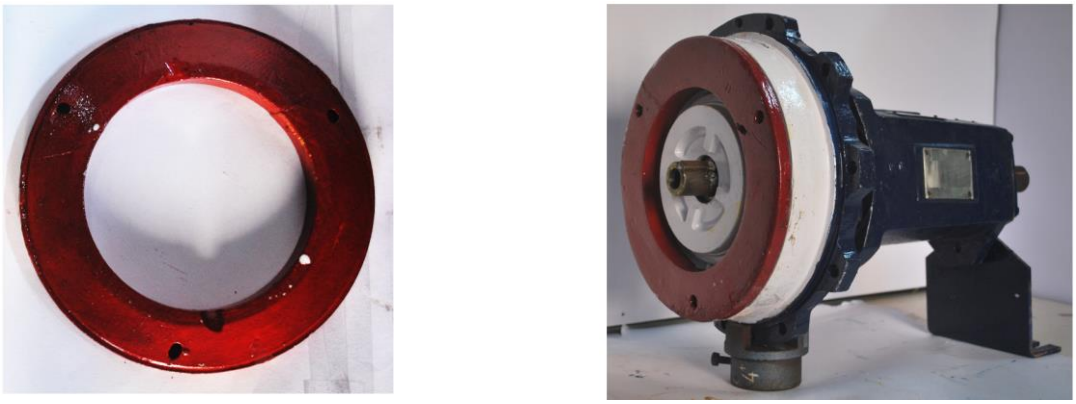

(a) (b)

Fig. 11 Actual experimental view of (a) manufactured cavity filling ring and (b) attachment of ring on back cover plate

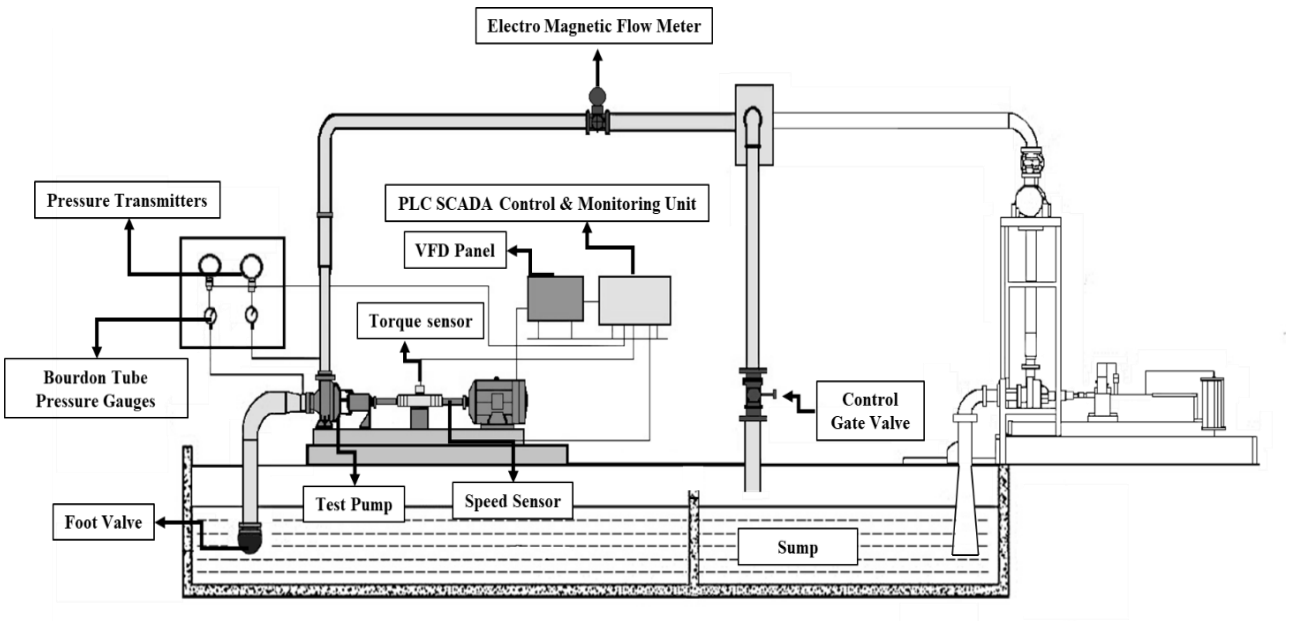

Fig. 12 Schematic diagram of the open-loop test bench

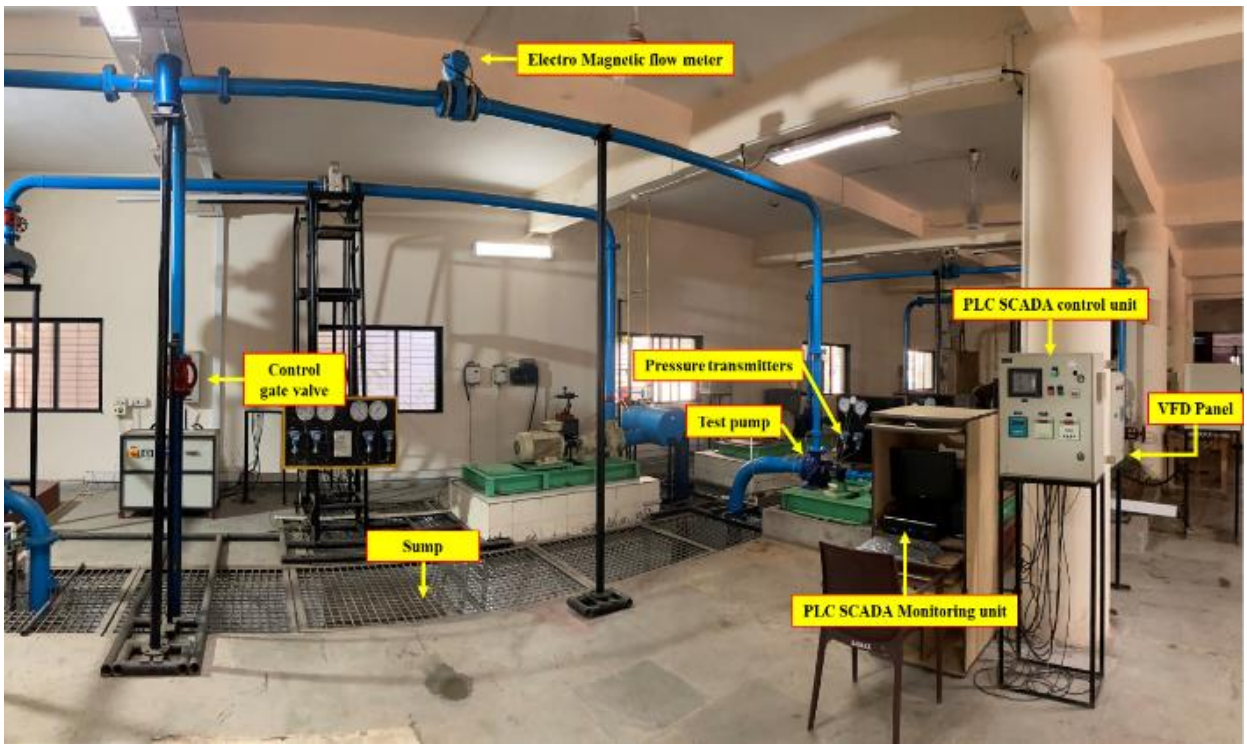

Fig. 13 Actual experimental view of the open loop test bench

depicted in Fig. 13. To measure the Q of the pump 0 to 60 lps ranged an electromagnetic flowmeter (Endress+Hauser-Promag 10 make) with accuracy of ±0.5% FS was used. For the evaluation of the H, 0 to 780 mm of Hg ranged pressure transmitter (Honeywell/ST-700 make) was installed at inlet of the pump while -14.7 to 500 PS ranged another pressure transmitter installed at the outlet of the pump with an accuracy of ±0.065% FS for both transmitters. The pump out-flow was controlled with a control gate valve. The rotating speed of the model pump was controlled by a variable frequency drive (VFD) unit connected with the electrical motor of the pump. Non-contact type rotary torque sensor (Honeywell-1703 make) with an accuracy of ±0.25% was utilized to measure the input T. To measure the N of the pump, a speed sensor was installed on the setup. The flowmeter and pressure transmitters were calibrated by comparing it using standard temperature/electrical calibrator as well as pressure calibrator, while torque sensor was calibrated against dead weight torque test rig with calibrated lever arm and SS force weights. The input power (P_i) of the pump was measured by neglecting the electrical motor, VFD drive, and transmission losses. A programmable logic controller (PLC) supported by supervisory control and data acquisition (SCADA) software was integrated into the system for effective monitoring and accurate data collection of the flow rate and pressure measurements. The power input (P_i), power output (P_o), and η is calculated using following equations (Stepanoff, 1957):

$$P_i = \frac{2\pi NT}{60000} \tag{4}$$

$$P_o = 9.81 \times Q \times H \tag{5}$$

$$\eta = \left(\frac{P_o}{P_i}\right) \times 100 \tag{6}$$

For the accurate evaluation of the Model A and Model B performance, the experiments were performed for various rotational speeds 1000, 900, and 800 rpm. To cover the complete operating range of Q, the operating valve was opened fully for highest flow rate ($Q_{\max}$) to the partial closing off the valve until the minimum flow rate ($Q_{\min}$ = 5 lps) as per manufacturer's pump data. Total of 153 test runs were performed in three sets to determine the repeatability in results at 1000 (total of nineteen Q), 900 (total of seventeen Q), and 800 rpm (total of fifteen Q) for data collection accuracy. In this section, the arithmetic mean value of the performance parameters (H, T and η) was considered for comparison. The change in performance parameters between Model A and Model B were evaluated and compared at respective Best Efficiency Point (BEP). Additionally for better comparison, the disk friction coefficient (C_m) and P_L due to L_{DF} are calculated as follows (Poullikkas, 1995):

$$C_m = \left(\frac{k}{R}\right)^{0.25} \frac{\left(C_{s,a,r}/R\right)^{0.1}}{{R_e}^{0.2}} \tag{7}$$

$$P_L = C_m \times \rho \times \omega^3 \times R^5 \tag{8}$$

The statistical internal uncertainty associated with the performance parameters were ended up in the range of ±10%.

4. Comparison and Validation of CFD and Experimental Results

4.1 Experimental Results

Figure 14, 15, and 16 shows the variation in H, T and η vs Q for 1000, 900, and 800 rpm to compare the Model B with Model A. As the Q increases, the H reduces and T increases for particular rpm following linear trend for both

Table 1 Experimental percentage improvement in H, reduction in input T and enhancement in η at Q_{max}, Q_{BEP} and Q_{min} conditions for all rpms

Performance Variation (in %)	Rotational Speed (in rpm)	Flow Conditions (in lps)		
		Q_{max}	Q_{BEP}	Q_{min}
H (↑)	1000	9.11	3.43	3.72
	900	4.83	1.79	1.13
	800	3.23	0.76	0.41
T (↓)	1000	0.12	0.47	0.61
	900	0.56	1.39	1.86
	800	1.21	2.32	3.14
η (↑)	1000	8.93	3.94	4.20
	900	5.47	3.91	3.93
	800	4.23	2.81	3.31

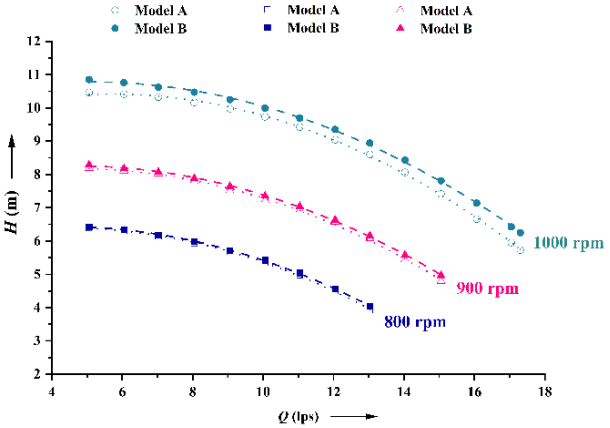

Fig. 14 H vs Q curve for 1000, 900 and 800 rpm

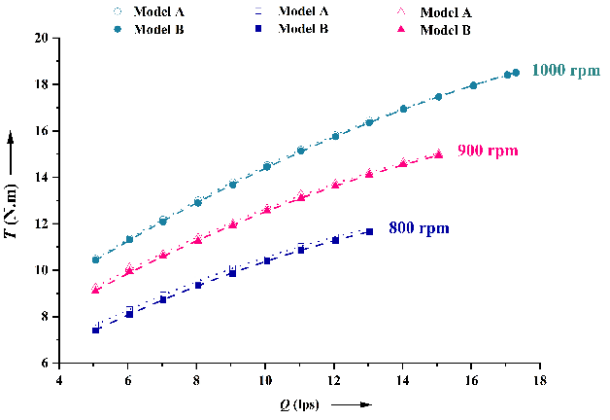

Fig. 15 T vs Q curve for 1000, 900 and 800 rpm

Model A and Model B. While, η increases till respective BEP and then reduces. Also, as the rpm increases from 800 to 1000 rpm, H, T and η has higher values at constant Q for both the models. One can observe that at 1000 rpm performance of pump improves reasonably in Model B in compare to Model A at any constant Q. Also, the pump exhibits the maximum enhancement in performance parameters at Q_{max} in order of Q_{BEP}, and Q_{min}.

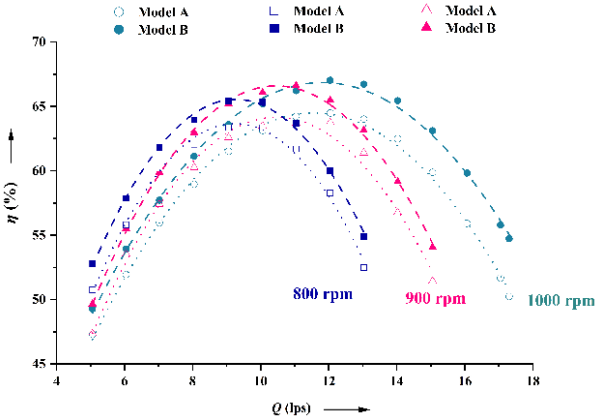

Fig. 16 η vs Q curve for 1000, 900 and 800 rpm

These can be understood as for the Model A, clearance flow in $C_{s,a,r}$ at the impeller entrance generates the high-speed leakage to strike with low speed mainstream. This collision results in vortices and generates the reverse flow. This flow reversal obstructs the freely flow of the impeller and increases the input T. In addition, these vortices formation disrupts the operation of the pump near the fluid mixing zone creating more H loss. In Model B, lower $C_{s,a,r}$ restricts the re-entrance of the fluid in volute reduces the flow separation and maintain the more uniform smooth flow reducing the input T. Also, reduction in recirculation of fluid imparts more efficient transfer of hydraulic energy from the impeller leading to the improved H. These increment in H and decrement in T, ultimately enhances the η. The percentage improvement in H, reduction in input T and enhancement in η at Q_{max}, Q_{BEP}, and Q_{min} conditions for all rpms is represented in Table 1.

Figure 17 shows the variation in C_m for a range of $C_{s,a,r}/R$ starting from 0.177 at $C_{s,a,r}$ = 23 mm to 0.008 for at $C_{s,a,r}$ = 1 mm for all the rpms. The variation curve illustrates the same inline trend curve for all the rpms until the theoretical boundary layer thickness of the impeller ($C_{s,a,r}/R$ = 0.06). Further for a constant $C_{s,a,r}/R$, the C_m reduces slightly as the speed of the pump varies from 800 rpm to 1000 rpm. The effect of C_m on energy loss analysis using the P_L is displayed in Fig. 18. The variation in P_L

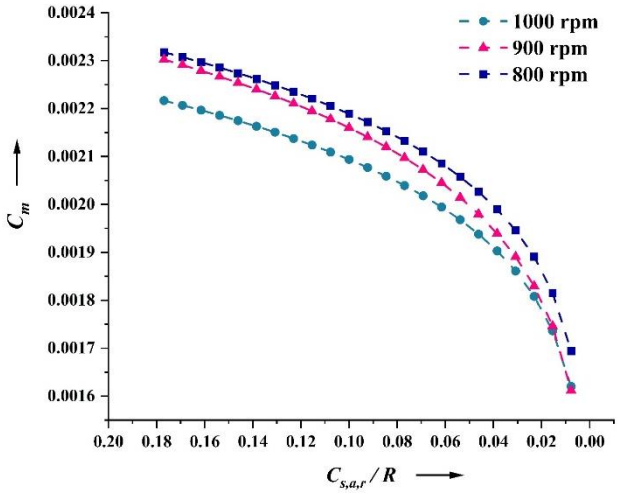

Fig. 17 C_m vs $C_{s,a,r}/R$ curve for 1000, 900 and 800 rpm

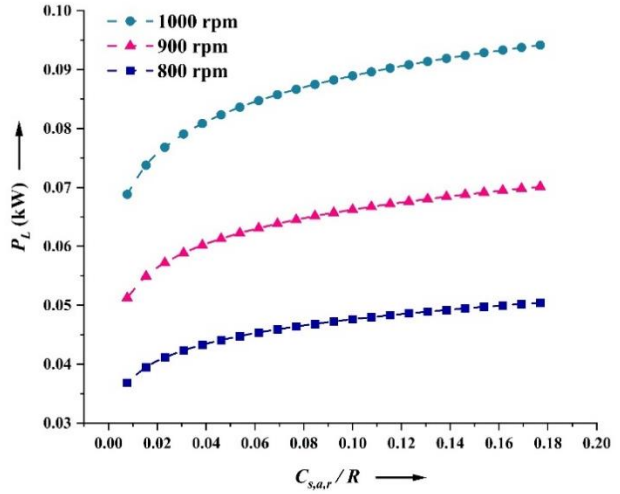

Fig. 18 P_L vs $C_{s,a,r}/R$ curve for 1000, 900 and 800 rpm

with $C_{s,a,r}/R$ follows the same trend curve of C_m as shown in Fig. 17. Also, as the speed of the pump varies from 800 rpm to 1000 rpm, P_L increases which is evidential from the Eq. (2). However, the deviation in P_L for over a whole range of $C_{s,a,r}/R$ at all rpms is similar (~26.91%). This study demonstrates how increases in $C_{s,a,r}/R$ cause the recirculation region to widen, which in turn causes increases in L_{DF}. Moreover, because of the wall's viscous effect, the recirculation area was reduced to a smaller extent than the boundary layer thickness, which results in increases in L_{DF}.

4.2 Validation of CFD Results

To verify the accuracy of the CFD model, the performance characteristic curve for Model A at 1000 rpm is compared with the experimental observations as shown in Fig. 19. Both the CFD and experimental curves displays the same trend for all the performance parameters which is in line with the classical theory of turbomachinery. Average differential percentage in H, T and η were found to be 2.8%, 3.6%, and 3.9%, respectively. For better comparison, percentage change in head ($\%\Delta H$) and

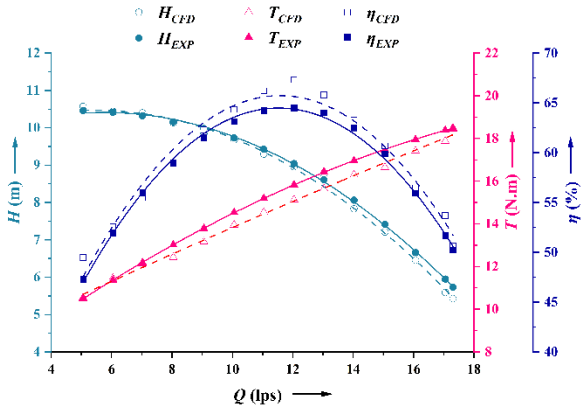

Fig. 19 Model A performance characteristic curve for 1000 rpm

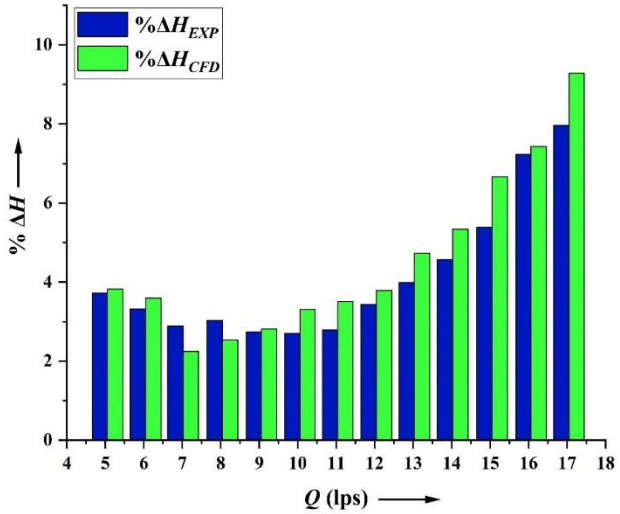

Fig. 20 $\%\Delta H$ variation for 1000 rpm

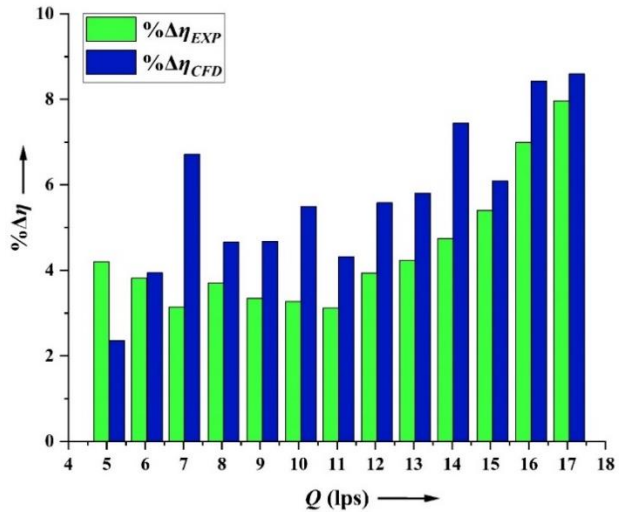

Fig. 21 $\%\Delta\eta$ variation for 1000 rpm

($\%\Delta\eta$) in Model B compare to Model A are represented in Fig. 20 and 21 respectively. The $\%\Delta H$ in CFD and experimental observations are almost similar while $\%\Delta\eta$ are large in CFD results. This can be understood as

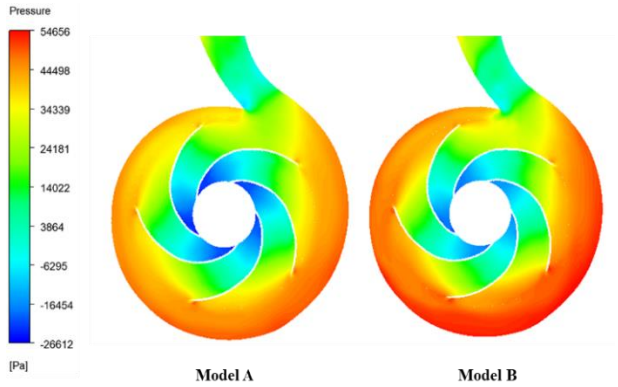

(a)

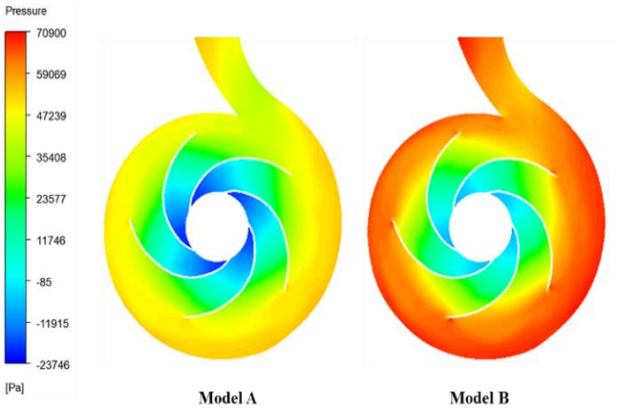

(b)

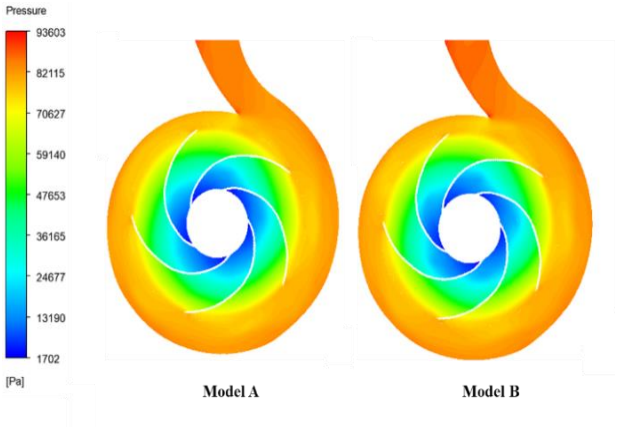

(c)

Fig. 22 Pressure contours in the middle section of pump at 1000 rpm for (a) Q_{max}, (b) Q_{BEP} and (c) Q_{min}

developed Model B in CFD completely ignores the fluid flow loss caused by the clearance flow in the pump while during the experiments there were some losses may still occur however small $C_{s,a,r}$ may be. These good agreements in results for both the models ensure the accuracy of CFD simulation for more detailed internal flow field analysis.

4.3 Internal Flow Field Analysis

For the better understanding of the clearance flow phenomena due to lowering the $C_{s,a,r}$ and subsequently reducing the L_{DF} on performance of pump, various tools available in flow field analysis of CFD are used. Figure 22 and 23 shows the static pressure distribution in the middle and end span of the pump at different flow rate conditions (Q_{max}, Q_{BEP} and Q_{min}) for Model A and B at 1000 rpm. As the flowrate reduces, the pressure in the pump gradually improves from the impeller inlet to the outlet of volute increasing the H for both the models which is mainly reflected in the value. The increase in pressure rise was continuously seen in all important zones, including the rear clearance area (at Q_{max} = 17.96%, Q_{BEP} = 27.58% and Q_{min} = 2.37%), and impeller departure (at Q_{max} = 11.25% , Q_{BEP} = 33.82% and Q_{min} = 1.04%), rather than being restricted to any one place. In comparison of Model B to Model A, the pressure increment distribution was much smoother at Q_{BEP} () compared to the Q_{max} and Q_{min}. Further, the local pressure distribution in the volute was relatively disordered for Q_{max} and Q_{min} conditions. A similar phenomena was noted by various researchers (Majidi, 2005; Zhou et al., 2013; Gao et al., 2014).

The absolute velocity distribution in the middle and end span of the pump at different flow rate conditions (Q_{max}, Q_{BEP} and Q_{min}) for Model A and B at 1000 rpm is depicted in Fig. 24 and 25. The velocity reduction in the rear clearance area (at Q_{max} = 83.23% , Q_{BEP} = 93.75% and Q_{min} = 58.96%), and impeller departure area (at Q_{max} = 19.36% , Q_{BEP} = 16.94% and Q_{min} = 22.5%) was obtained, respectively. Under various flowrates, the large difference in velocity distribution between impeller inlet and outlet was observed. Operating the pump from Q_{max} to Q_{min}, the velocity in the volute reduces. This reduced velocity attributes to the more conversion of kinetic energy into potential energy in terms of pressure and head, which is evidential from Figure 22 and 23. Also, due to the reduction in interference effect at the impeller outlet flow separation was reduced.

To get the clearer picture about the performance improvement, velocity vectors and streamline distribution in the upper half of end span of the pump at different flow rate conditions (Q_{max}, Q_{BEP} and Q_{min}) for Model A and B at 1000 rpm is depicted in Fig. 26 and 27. The fluid is transported radially outward by centrifugal forces created by the impeller's rotational motion. However, because of continuity, the fluid flow creates a circulating flow in the $C_{s,a,r}$ as it returns radially inward along the casing wall in Model A. Large $C_{s,a,r}$ causes the water flow to become turbulent and the boundary layer to split which generates the core flow in back clearance space. While in the Model B for all the flow rate conditions, the flow separation in the clearance space was reduced indicating the positive effect on the mainstream of the pump. Also, the smoothness of the flow in Model B imparts the reduction in impaction effect at the tongue of the volute shows the improvement in performance. At the same time, the front side clearance space's velocity decreased in magnitude. As a result, the experimental results show that the boundary layer that is thrown off the shroud can transmit its energy to the main flow, which will ultimately result in an increase in delivery pressure as shown in Fig. 22 and 23 while reduction in velocity as shown in Fig. 24 and 25.

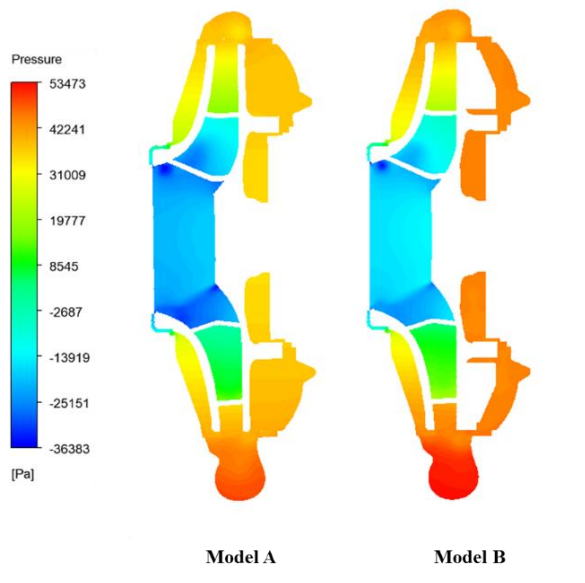

(a)

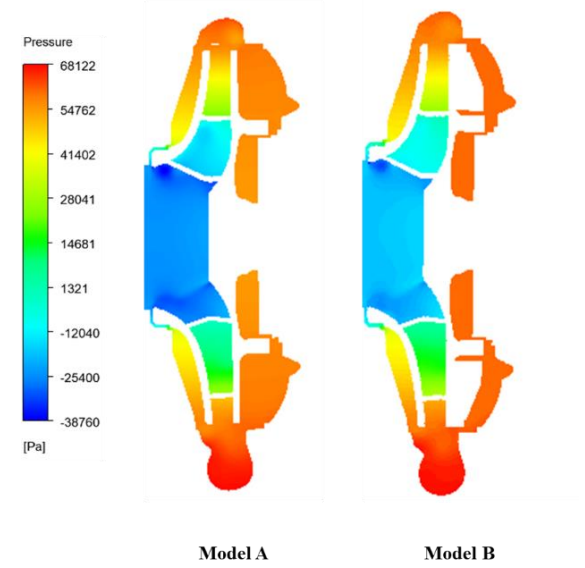

(b)

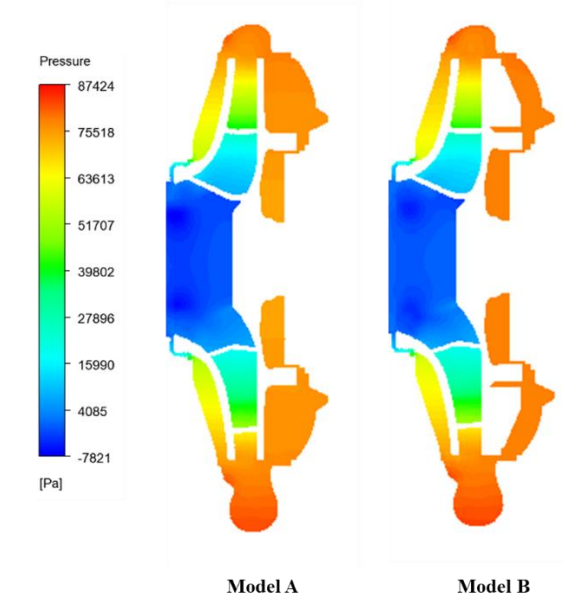

(c)

Fig. 23 Pressure contours in the end section of pump at 1000 rpm for (a) Q_{max}, (b) Q_{BEP} and (c) Q_{min}

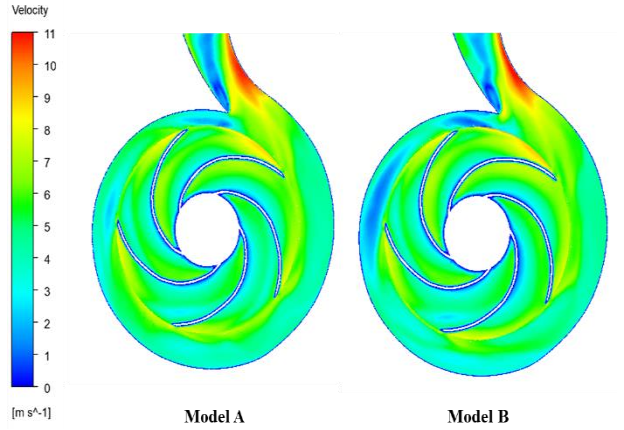

(a)

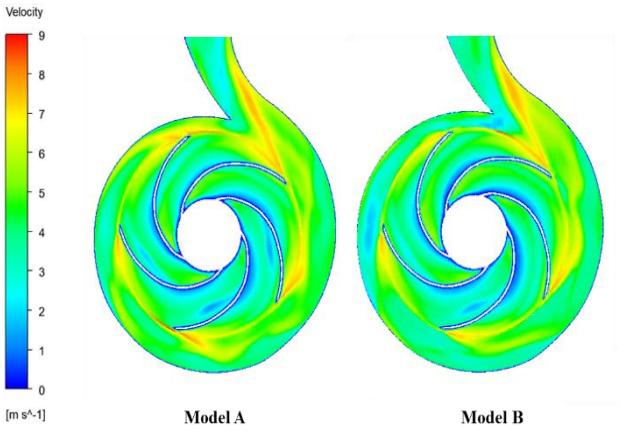

(b)

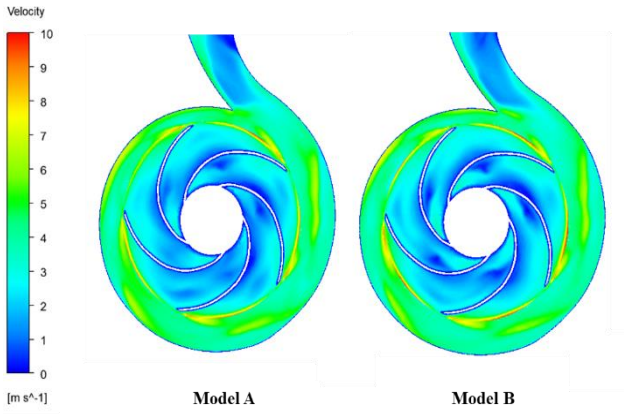

(c)

Fig. 24 Velocity contours in the middle section of pump at 1000 rpm for (a) Q_{max}, (b) Q_{BEP} and (c) Q_{min}

5. CONCLUSION

Experimental and CFD investigation of the lower N_s pump was done to investigate the effect of reduction in L_{DF} by lowering the $C_{s,a,r}$. Model A with original $C_{s,a,r}$ of 23 mm and Model B with reduced $C_{s,a,r}$ of 1 mm were evaluated at different rpms (1000, 900 and 800 rpm) and at various flow rates. From the both experimental and CFD analysis tools as well as flow field analysis following conclusions have been drawn:

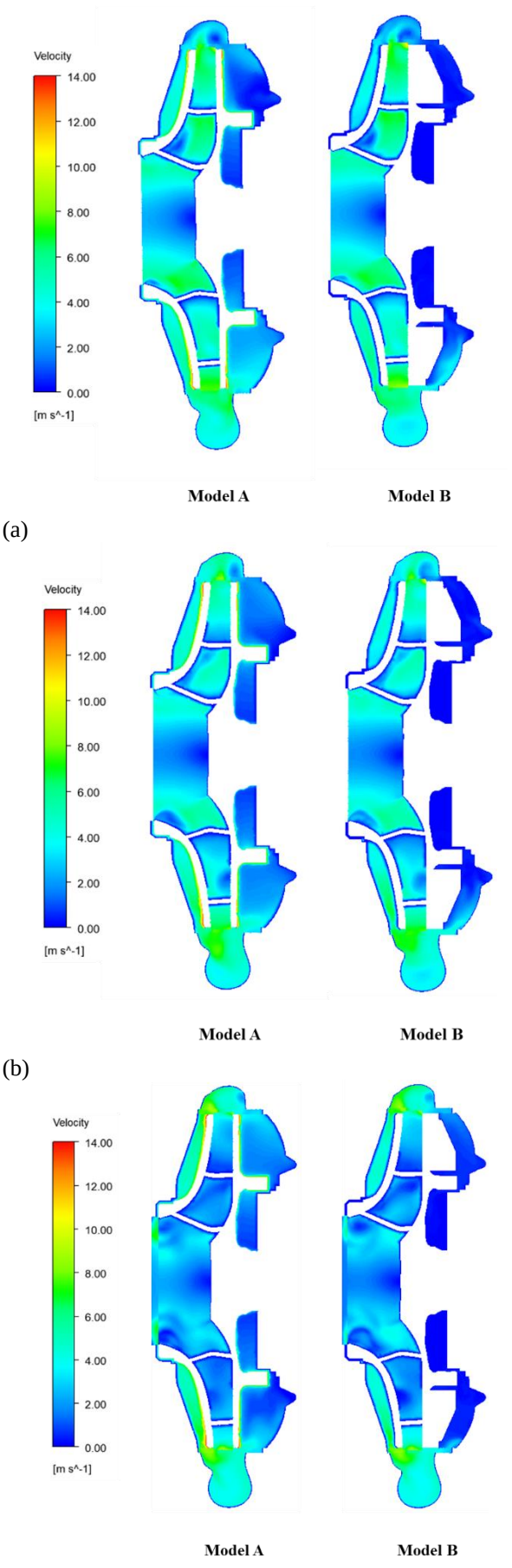

Fig. 25 Velocity contours in the middle section of pump at 1000 rpm for (a) Q_{max}, (b) Q_{BEP} and (c) Q_{min}

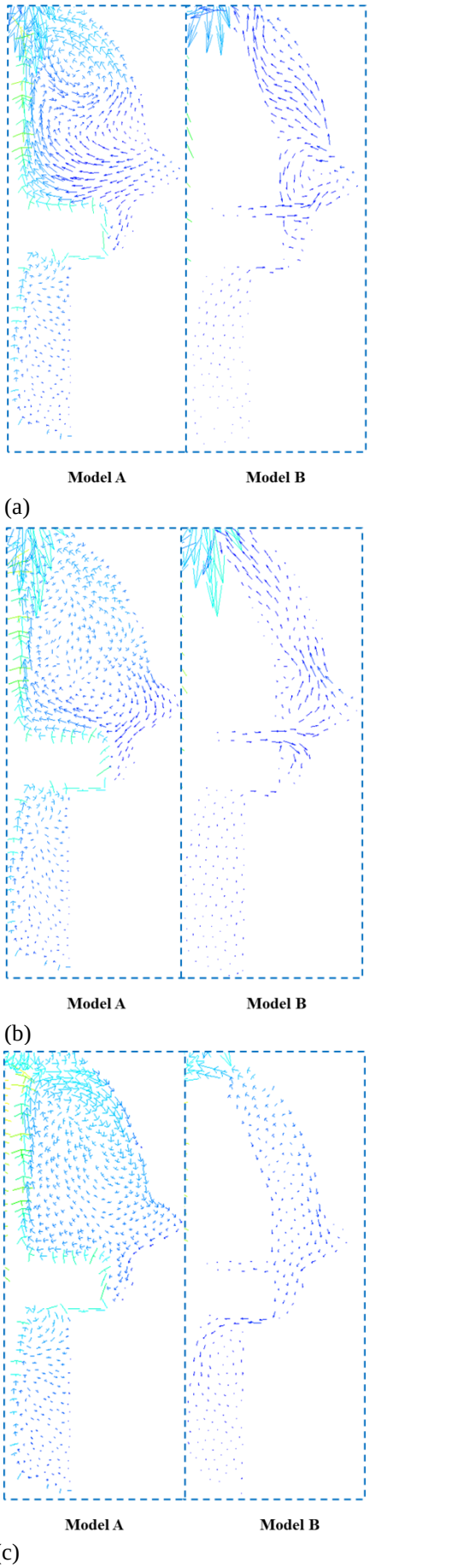

Fig. 26 Velocity vectors in the end section upper half of pump at 1000 rpm for (a) Q_{max}, (b) Q_{BEP} and (c) Q_{min}

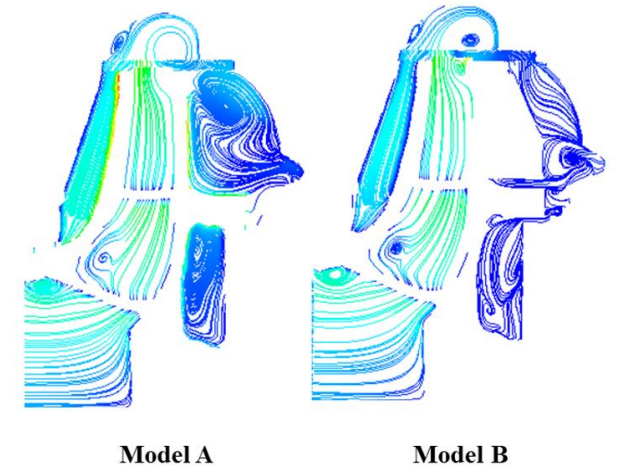

(a)

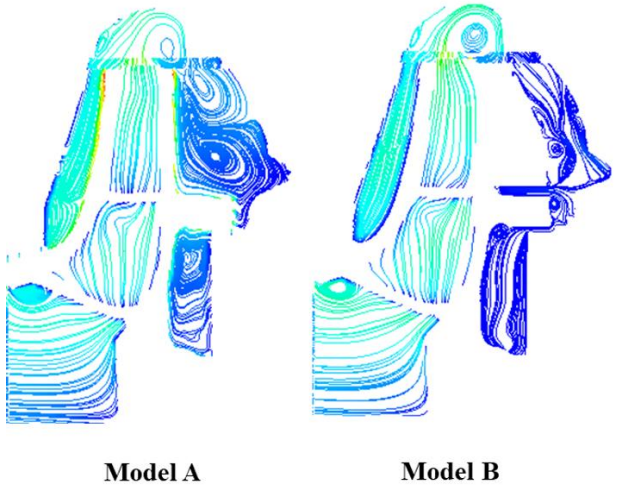

(b)

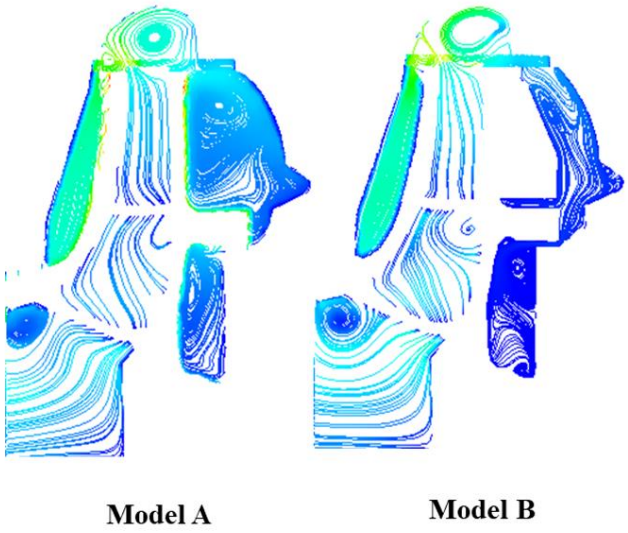

(c)

Fig. 27 Streamline distribution in the end section upper half of pump at 1000 rpm for (a) Q_{max}, (b) Q_{BEP} and (c) Q_{min}

- In comparison of Model A, Model B exhibits the great performance improvement in both the analysis. As the $C_{s,a,r}$ is reduced in Model B, the reverse clearance flow is restricted leading to the less entrapment and more uniform pattern fluid flow which increases the conversion rate of kinetic energy to pressure energy. This efficient conversion improves H and η for all the rpms over a range of flow rate, while reduces the required input T. The average improvement in H was 4.49%, 1.85% and 1.31% while in η 4.77%, 3.59% and 2.98% was observed in Model B in compare of Model A, for 1000, 900 and 800 rpm respectively.
- In compare to the other rpms, Model B observes higher rise in the hydraulic performance parameters (9.11% H and 8.93% η) at 1000 rpm for Q_{max} condition. Further, the performance of both the models were enhanced as the flow rate varies from Q_{max} to Q_{BEP} to Q_{min}. These can be mainly due to the decrement in recirculation area than the boundary layer thickness resulting in reduction in L_{DF} at higher rpm. Also, flow filed analysis supports these phenomena through increment in pressure and decrement in velocity from impeller outlet to volute outlet region.
- The strong agreement between the experimental and CFD results of the current research activity regarding the pump's hydraulic performances suggests that the suggested Model B can capture most of the spatial flow pattern in the test pump and improvement in hydraulic parameters.
- Although, the current research focuses on improvement in lower N_s centrifugal pump performance, other types of pumps needed to be explored and compared with reduced $C_{s,a,r}$. Also, other possibilities such as variation in design of impeller, back cover plate, more polished and smooth surfaces to reduce the L_{DF} using different working fluids can be researched.

In conclusion, this study can serve as a useful guide for comprehending, evaluating, and managing the mechanisms underlying the intricate phenomena occurring in clearance flow in lower $\boldsymbol{N_s}$ centrifugal pumps, particularly when they are running at low flow rates and higher speed. This design advances beyond theoretical or computational approaches by offering a straightforward modification that can be retrofitted into existing pump systems. The approach not only enhances pump efficiency and head performance but also addresses real-world challenges in energy efficiency. With centrifugal pumps consuming a significant portion of global electricity, this innovation has the potential to create substantial energy savings and reduce greenhouse gas emissions, especially in industrial, municipal, and agricultural applications. Its scalability and impact make it a transformative step in pump system optimization.

CONFLICT OF INTEREST

The authors declare that they have no known competing financial interests or personal relationships that

could have appeared to influence the work reported in this paper.

AUTHORS CONTRIBUTION

Dokiparti Satish: Numerical Simulation, Experimentation, Methodology, Validation, Investigation, Analysis, Writing - Original Draft, Review and Editing. **Ashish Doshi**: Conceptualization, Methodology, Investigation, Resources, Supervision. **Mukund Bade**: Methodology, Investigation, Resources, Supervision.

REFERENCES

Abernethy, R. B., Benedict, R. P., & Dowdell, R. B. (1985). ASME measurement uncertainty. *Journal of Fluids Engineering, Transactions of the ASME*, *107*(2), 161–164. https://doi.org/10.1115/1.3242450

Adistiya, S., & Wijayanta, A. T. (2019). *Effect of clearance gap on hydraulic efficiency of centrifugal pump*. AIP Conference Proceedings, 2097. https://doi.org/10.1063/1.5098228

Ahmed, H., & Creamer, J. (2024). *Why Pumping Infrastructure Matters*. https://empoweringpumps.com/schneider-electric-pumping-infrastructure-matters/

Ayad, A. F., Abdalla, H. M., & El-Azm Aly, A. A. (2015). Effect of semi-open impeller side clearance on the centrifugal pump performance using CFD. *Aerospace Science and Technology*, *47*, 247–255. https://doi.org/10.1016/j.ast.2015.09.033

Badami, M. (1997). Theoretical and experimental analysis of traditional and new periphery Pumps. *SAE Technical Papers*. https://doi.org/10.4271/971074

Cao, L., Zhang, Y., Wang, Z., Xiao, Y., & Liu, R. (2015). Effect of axial clearance on the efficiency of a shrouded centrifugal pump. *Journal of Fluids Engineering, Transactions of the ASME*, *137*(7). https://doi.org/10.1115/1.4029761

Celik, I. B., Ghia, U., Roache, P. J., Freitas, C. J., Coleman, H., & Raad, P. E. (2021). Procedure for estimation and reporting of uncertainty due to discretization in CFD applications. *Journal of Fluids Engineering, Transactions of the ASME*, *130*(7), 0780011–0780014. https://doi.org/10.1115/1.2960953

Chen, B., Yu, L., Li, X., & Zhu, Z. (2024). Insights into turbulent flow structure and energy dissipation in centrifugal pumps: A study utilizing time-resolved particle image velocimetry and proper orthogonal decomposition. *Ocean Engineering*, *304*. https://doi.org/10.1016/j.oceaneng.2024.117903

Choi, W. C., Yoo, I. S., Park, M. R., & Chung, M. K. (2013). Experimental study on the effect of blade angle on regenerative pump performance. *Proceedings of the Institution of Mechanical Engineers, Part A: Journal of Power and Energy*, *227*(5), 585–592. https://doi.org/10.1177/0957650913487731

Gao, Z., Zhu, W., Lu, L., Deng, J., Zhang, J., & Wuang, F. (2014). Numerical and experimental study of unsteady flow in a large centrifugal pump with stay vanes. *Journal of Fluids Engineering, Transactions of the ASME*, *136*(7). https://doi.org/10.1115/1.4026477

Gülich, J. F. (2003). Disk friction losses of closed turbomachine impellers. *Forschung Im Ingenieurwesen/Engineering Research*, *68*(2), 87–95. https://doi.org/10.1007/s10010-003-0111-x

Gülich, J. F. (2019). *Centrifugal pumps*. Fourth Edition. Centrifugal Pumps, Fourth Edition. Springer International Publishing. https://doi.org/10.1007/978-3-030-14788-4

Horiguchi, H., Wakiya, K., Tsujimoto, Y., Sakagami, M., & Tanaka, S. (2008). Study for the increase of micro regenerative pump head. *Nihon Kikai Gakkai Ronbunshu, B Hen/Transactions of the Japan Society of Mechanical Engineers, Part B*, *74*(10), 2154–2162. https://doi.org/10.1299/kikaib.74.2154

IEA (2023). World Energy Outlook 2023 Free Dataset. In Https://Www.Iea.Org/Data-and-Statistics/Data. https://www.iea.org/reports/world-energy-outlook-2023

Inaba, Y., Sakai, K., Miyagawa, K., Iino, M., & Sano, T. (2021). Investigation of flow structure in a narrow clearance of a low specific speed centrifugal impeller. *Journal of Fluids Engineering, Transactions of the ASME*, *143*(12). https://doi.org/10.1115/1.4052240

Iversen, H. W. (1955). Performance of the periphery pump. *Journal of Fluids Engineering*, *77*(1), 19–22. https://doi.org/10.1115/1.4014210

Jin, F., Li, N., Wei, Z., Wu, Y., Tao, R., & Xiao, R. (2022). Sensitivity analysis on the influence factors of clearance axial force of a varying-speed centrifugal pump. *Journal of Physics: Conference Series*, *2217*(1). https://doi.org/10.1088/1742-6596/2217/1/012001

Kim, B., Siddique, M. H., Bellary, S. A. I., aljehani, A. S., Choi, S. W., & Lee, D. E. (2023). Investigation of a centrifugal pump for energy loss due to clearance thickness while pumping different viscosity oils. *Results in Engineering*, *18*. https://doi.org/10.1016/j.rineng.2023.101038

Li, X., Ouyang, T., Lin, Y., & Zhu, Z. (2023). Interstage difference and deterministic decomposition of internal unsteady flow in a five-stage centrifugal pump as turbine. *Physics of Fluids*, *35*(4). https://doi.org/10.1063/5.0150300

Maeda, S., Sano, T., Miyagawa, K., & Sakai, K. (2024). Reduction of disk friction loss by applying a fin to the back of a centrifugal impeller. *Journal of Fluids Engineering, Transactions of the ASME*, *146*(7). https://doi.org/10.1115/1.4065047

Majidi, K. (2005). Numerical study of unsteady flow in a centrifugal pump. *Journal of Turbomachinery*, *127*(2), 363–371. https://doi.org/10.1115/1.1776587

Osman, F. K., Zhang, J., Lai, L., & Kwarteng, A. A. (2022). Effects of turbulence models on flow characteristics of a vertical fire pump. *Journal of Applied Fluid Mechanics*, *15*(6), 1661–1674. https://doi.org/10.47176/jafm.15.06.1303

Pehlivan, H., & Parlak, Z. (2019). Investigation of parameters affecting axial load in an end suction centrifugal pump by numerical analysis. *Journal of Applied Fluid Mechanics*, *12*(5), 1615–1627. https://doi.org/10.29252/JAFM.12.05.29623

Peng, G., Hong, S., Chang, H., Fan, F., Zhang, Y., & Shi, P. (2022). Numerical and experimental research on the influence of clearance between impeller and cover on the pump performance. *Mechanika*, *28*(1), 67–72. https://doi.org/10.5755/j02.mech.28904

Poullikkas, A. (1995). Surface roughness effects on induced flow and frictional resistance of enclosed rotating disks. *Journal of Fluids Engineering, Transactions of the ASME*, *117*(3), 526–528. https://doi.org/10.1115/1.2817294

Raheel, M. M., & Engeda, A. (2005). Systematic design approach for radial blade regenerative turbomachines. *Journal of Propulsion and Power*, *21*(5), 884–892. https://doi.org/10.2514/1.1426

Shimosaka, M. (1959). Research on the characteristics of regenerative pump. Research on the Characteristics of Regenerative Pump : 2nd Report, Theoretical Performance. *Transactions of the Japan Society of Mechanical Engineers*, *25*(157), 951–959. https://doi.org/10.1299/kikai1938.25.951

Shirinov, A., & Oberbeck, S. (2011a). High vacuum side channel pump working against atmosphere. *Vacuum*, *85*(12), 1174–1177. https://doi.org/10.1016/j.vacuum.2010.12.018

Shirinov, A., & Oberbeck, S. (2011b). *Optimisation of the high vacuum side channel pump*. Institution of Mechanical Engineers - 7th International Conference on Compressors and Their Systems 2011, 81–92. https://doi.org/10.1533/9780857095350.2.81

Sixsmith, H. (1913). The theory and design of structures. *Nature*, *92*(2288), 4–4. https://doi.org/10.1038/092004c0

Stepanoff, A. J. (1957). Centrifugal and axial flow Pumps. *Journal of the Franklin Institute*, *264*(5). https://doi.org/10.1016/0016-0032(57)90043-1

Wilcox, D. A. (1994). Simulation of transition with a two-equation turbulence model. *AIAA Journal*, *32*, 247–255. http://arc.aiaa.org/doi/abs/10.2514/3.59994?journalCode=aiaaj

Wilcox, D. C. (1988). Reassessment of the scale-determining equation for advanced turbulence models. *AIAA Journal*, *26*(11), 1299–1310. https://doi.org/10.2514/3.10041

Will, B. C., Benra, F. K., & Dohmen, H. J. (2012). Investigation of the flow in the impeller side clearances of a centrifugal pump with volute casing. *Journal of Thermal Science*, *21*(3), 197–208. https://doi.org/10.1007/s11630-012-0536-3

Wilson, D. G. (1982). Turbomachinery - from paddle wheels to turbojets. *Mech. Engng.*, *104*(10, Oct. 1982), 28–40.

Zheng, L., Chen, X., Dou, H. S., Zhang, W., Zhu, Z., & Cheng, X. (2020). Effects of clearance flow on the characteristics of centrifugal pump under low flow rate. *Journal of Mechanical Science and Technology*, *34*(1), 189–200. https://doi.org/10.1007/s12206-019-1220-2

Zhou, L., Shi, W., Li, W., & Agarwal, R. (2013). Numerical and experimental study of axial force and hydraulic performance in a deep-well centrifugal pump with different impeller rear shroud radius. *Journal of Fluids Engineering, Transactions of the ASME*, *135*(10). https://doi.org/10.1115/1.4024894

Zhu, B., Chen, H. X., Wei, Q., & Zhang, R. (2012). The analysis of unsteady characteristics in the low specific speed centrifugal pump with drainage gaps. *IOP Conference Series: Earth and Environmental Science*, *15*(PART 3). https://doi.org/10.1088/1755-1315/15/3/032049